1 **In-cloud formation of secondary species in iron-containing**

2 **particles**

4 Qinhao Lin[1], Xinhui Bi[1,*], Guohua Zhang[1], Yuxiang Yang[1,2], Long Peng[1,2], Xiufeng Lian[1,2],

5 Yuzhen Fu[1,2], Mei Li[3], Duohong Chen[4], Mark Miller[5], Ji Ou[6], Mingjin Tang[1], Xinming

6 Wang[1], Ping'an Peng[1], Guoying Sheng[1], and Zhen Zhou[3]

8 [1] State Key Laboratory of Organic Geochemistry and Guangdong Key Laboratory of

9 Environmental Resources Utilization and Protection, Guangzhou Institute of Geochemistry,

10 Chinese Academy of Sciences, Guangzhou 510640, PR China

11 [2] University of Chinese Academy of Sciences, Beijing 100039, PR China

12 [3] Institute of Mass Spectrometer and Atmospheric Environment, Jinan University, Guangzhou

13 510632, PR China

14 [4] State Environmental Protection Key Laboratory of Regional Air Quality Monitoring,

15 Guangdong Environmental Monitoring Center, Guangzhou 510308, PR China

16 [5] Department of Environmental Sciences, Rutgers, the State University of New Jersey, New

17 Brunswick, NJ 08901, USA

18 [6] Shaoguan Environmental Monitoring Center, Shaoguan 512026, PR China

22 *Correspondence to: Xinhui Bi (bixh@gig.ac.cn)

24   **Abstract.** The increase of secondary species through cloud processing potentially increases

25   aerosol iron (Fe) bioavailability. In this study, a ground-based counterflow virtual impactor

26   coupled with a real-time single-particle aerosol mass spectrometer was used to characterize the

27   formation of secondary species in Fe-containing cloud residues (dried cloud droplets) at a

28   mountain site in southern China for nearly one month during the autumn of 2016. Fe-rich, Fe-

29   dust, Fe-elemental carbon (Fe-EC), and Fe-vanadium (Fe-V) cloud residual types were obtained

30   in this study. The Fe-rich particles, related to combustion sources, contributed 84% to the Fe-

31   containing cloud residues, and the Fe-dust particles represented 12%. The remaining 4%

32   consisted of the Fe-EC and Fe-V particles. It was found that extremely high amounts of sulfate

33   had already accumulated on the Fe-containing particles before cloud events, leading to no

34   distinct changes in sulfate during cloud events. Cloud processing contributed to the

35   enhancement of nitrate, chloride, and oxalate in the Fe-containing cloud residues. However, the

36   in-cloud formation of nitrate and chloride in the Fe-rich type was less obvious relative to the

37   Fe-dust type. The enhancement of oxalate in the Fe-rich cloud residues was produced via

38   aqueous oxidation of oxalate precursors (e.g., glyoxylate). Moreover, Fe chemistry involved in

39   the Fenton reaction further promoted the conversion of the oxalate precursors to oxalate during

40   cloud events, although the photolysis of Fe-oxalate complexes also existed in the Fe-rich cloud

41   residues. This work emphasizes the role of combustion Fe sources in participating in cloud

42   processing and has important implications for evaluating Fe bioavailability from combustion

43   sources during cloud processing.

44   Keywords: Fe-containing particles, oxalate, cloud residues, secondary species, cloud

45   processing, southern China

1 Introduction

Iron (Fe) is frequently detected in atmospheric aerosols. Aerosol Fe has an adverse effect on human health, causing issues such as DNA strand breakage and cell damage (See et al., 2007; Abbaspour et al., 2014). Some researchers also reported that aerosol Fe solubility might be an important criterion for toxicity in lung fluid (Costa and Dreher, 1997). Bioavailable Fe derived from atmospheric aerosol deposition can limit the photosynthetic activity of marine phytoplankton in high-nutrient low-chlorophyll waters, indirectly affects oceanic carbon uptake and storage, and has feedback effects on climate (Jickells et al., 2005). Fe-containing aerosol particles contained various species, such as calcium (Ca), silicon (Si), aluminum (Al), vanadium (V), elemental carbon (EC), secondary inorganic and organic species (Zhang et al., 2014; Bi et al., 2016; Dall'Osto et al., 2016). The presence and coexistence of various species could further modify the effects of aerosol Fe on human health, ecology, and climate (Mahowald et al., 2005; Abbaspour et al., 2014).

Aerosol Fe sources mainly include mineral dust and combustion emissions (e.g., biomass burning, coal combustion, and iron/steel industrial activities) (Jickells et al., 2005; Sedwick et al., 2007). Abundant Ca, Si, and Al often exist in aerosol Fe from mineral dust sources (Sullivan et al. 2007), while aerosol Fe from combustion sources usually contains EC and other metals, as well as minor amounts of Ca (Li et al., 2013; Dall'Osto et al., 2016). The chemical properties of aerosol Fe depend on its emission sources and could also be modified by the formation of secondary species during atmospheric processes (Zhang et al., 2014; Dall'Osto et al., 2016; Lin et al., 2017). Aerosol Fe in East Asian outflows was often observed to be internally mixed with sulfate, mostly due to the large amount of SO_2 from coal in China (Furutani et al., 2011; Moffet

68   et al., 2012; Li et al., 2013). Sullivan et al. (2007) proposed that the enrichment of sulfate in the

69   Asian mineral dust was possibly due to the Fe-catalyzed oxidation of SO_2 to sulfate. In

70   European urban areas, Dall'Osto et al. (2016) found that aerosol Fe was internally mixed with

71   nitrate rather than sulfate, and was most likely associated with urban traffic activities. The

72   frequent measurement of oxalate in the aerosol Fe was produced via photochemical and/or

73   aqueous oxidation over East Asia (Sullivan and Prather 2007; Yang et al, 2009; Cheng et al,

74   2017).

75   The above observations about atmospheric processes of aerosol Fe were mainly performed

76   in environments with low relative humidity. Cloud processing accompanied by high amounts

77   of water played a vital role in the formation of secondary species (e.g., sulfate, nitrate, chloride,

78   ammonium, and oxalate) through the partitioning of gas-into-aqueous phases or

79   heterogeneous/multiphase processes (Sellegri et al. 2003; Lim et al., 2010; Chang et al., 2011;

80   Harris et al., 2013). For example, one model study had estimated that up to 80% of the total

81   production of sulfate globally originated from aqueous reactions (Tsai et al., 2010). The

82   presence of Fe in cloud droplets also allowed the conversion of SO_2 to sulfate via Fe-catalyzed

83   autoxidation reactions (Harris et al., 2013). Furthermore, Fe chemistry involved in Fenton or

84   Fenton-like reactions in cloud droplets yielded OH-radicals that can induce the conversion of

85   glyoxylic acid to low volatility organic aerosols (e.g., oxalate) (Ervens et al., 2011). Variable

86   alkaline species or organic precursors from different aerosol Fe types might affect the in-cloud

87   formation of secondary species. However, research on the effects of cloud processing on the

88   formation of secondary species in various aerosol Fe types remains poorly understood.

89   In this study, we used technology combining a ground-based counterflow virtual impactor

90   (GCVI) coupled with a real-time single-particle aerosol mass spectrometer (SPAMS) to obtain

91   information on the characteristics and potential sources of Fe-containing cloud residues at a

92   mountain site in southern China. Additionally, Fe-containing interstitial (non-activated particles)

93   and cloud-free particles were also analyzed. The impact of cloud processing on the formation

94   of sulfate, nitrate, chloride, ammonium, oxalate precursors, and oxalate in various Fe-

95   containing particle types were addressed.

96

97   **2 Experimental section**

98   **2.1 Sampling site**

99   The sampling site was situated in the Nanling Background Station (112°53'56'' E, 24°41'56''

100   N, 1690 m a.s.l.) in southern China. The measured area was in an acid precipitation region

101   (Annual Environment Report of China in 2016, http://www.mep.gov.cn/hjzl/). Due to the site

102   being surrounded by a national park forest (273 km^2), it was minimally affected by local

103   anthropogenic activities. However, it might be subjected to polluted air masses from the

104   southern Pearl River Delta city groups or from northern China (Lin et al. 2017). A detailed

105   description of the sampling site can be found elsewhere (Lin et al. 2017).

106

107   **2.2 Instrumentation**

108   Cloud droplets with an aerodynamics diameter greater than 8 μm were collected using a GCVI

109   inlet system (GCVI Model 1205, Brechtel Manufacturing Inc.). The collected cloud droplets

110   were dried using an evaporation chamber (airflow temperature at 40 °C) in the GCVI until only

111   dry residual particles (cloud residues) remained. To reliably guarantee the presence of cloud

112   events, an upper-limit visibility threshold of 5 km and a lower-limit RH threshold of 95% were

113   set in the GCVI software (Bi et al., 2016; Lin et al., 2017). During precipitation periods, the

114   GCVI automatically shut down to protect against interference from raindrops. The particle

115   transmission efficiency of the cut size (8 μm) was 50% (Shingler et al., 2012). Due to the cloud

116   droplets being concentrated in the GCVI inlet, an enrichment factor was estimated to be 5.25

117   based on theoretical calculations (Shingler et al., 2012). More detailed information about the

118   GCVI has been described in Bi et al. (2016). The number concentration of particles collected

119   by the GCVI was below 1 cm^3 during cloud-free periods, suggesting that instances of particle

120   breakthrough and small particle contamination were absent (Shingler et al., 2012). In addition,

121   interstitial particles or cloud-free particles were sampled using an inlet with a cut-off

122   aerodynamic diameter of 2.5 μm during cloudy or cloud-free episodes. The measurement

123   campaign was conducted from 9 October to 4 November, 2016. The time for cloud events was

124   approximately 300 hours in the whole period. The measurement period of cloud residues,

125   interstitial particles, and cloud-free particles are shown in Figure S1.

126   The sampled cloud residues, interstitial particles, and cloud-free particles were subsequently

127   measured by a single particle aerosol mass spectrometer (SPAMS) (Hexin Analytical

128   Instrument Co., Ltd., Guangzhou, China) to obtain their size-resolved chemical composition.

129   Bipolar mass spectra of individual aerosol particles were obtained by the SPAMS. The

130   analytical method of the SPAMS has been described in Li et al. (2011). Briefly, the aerosol

131   particles are focused into a narrow particle beam and accelerated to a region where the vacuum

132   aerodynamic (d_{va}) size of the aerosol particles is measured using two continuous diode Nd:YAG

133   laser beams (532 nm). Based on the light scattered by the particles, a pulsed high power laser

134   (266 nm) can be precisely triggered to evaporate and ionize the particles. Production of positive

135   and negative fragment is subsequently recorded using a dual-polarity time-of-flight mass

136   spectrometer. A specific mass-to-charge ratio (m/z) in the mass spectral corresponding to the

137   most probable ions is dependent on previous field and lab studies, and the peak area of a given

138   m/z on each particle is relevant to the amount of the corresponded species (Bhave et al., 2002;

139   Pratt et al., 2011). Polystyrene latex spheres (Nanosphere Size Standards, Duke Scientific Corp.,

140   Palo Alto) of 0.2-2.0 μm in diameter were used to calibrate the sizes of the detected particles at

141   the sampling site.

142

143   **2.3 Screening of the Fe-containing aerosols**

144   During the sampling period, 154,862 cloud residues, 15,420 interstitial particles, and 168,427

145   cloud-free particles with d_{va} ranged between 0.2 and 2.0 μm were chemically analyzed with

146   bipolar ion mass spectra. The Fe-containing aerosols typically had a positive ion peak at m/z

147   56. Because the Fe ion peak at m/z 56 may be contaminated with other species in the atmosphere,

148   such as $[CaO]^+$, $[KOH]^+$, and $[C_3H_4O]^+$, the natural isotopic composition of Fe ion peaks at

149   both m/z 54 and 56 were selected for the Fe screening process to minimize the interference

150   from other species (Furutani et al., 2011; Zhang et al., 2014). A peak area ratio $^{56}Fe/^{54}Fe > 10$

151   was also applied to strengthen the screening through excluding more ambiguous assignments

152   (Zhang et al., 2014; Dall'Osto et al., 2016). Thus, 5,682 cloud droplet residues, 395 interstitial

153   particles, and 5,086 cloud-free particles were found to be internally mixed with Fe, representing

154   3.7% of the total cloud residues, 2.6% of the total interstitial particles, and 3.0% of the total

155   cloud-free particles, respectively. Because the low number of the collected Fe-containing cloud

156   residues limited the statistical analysis, the differences between single cloud events were not

157   analyzed. Instead, an average analysis covering all the cloud events was presented.

158   The Fe-containing aerosols, including cloud residues, interstitial particles, and cloud-free

159   particles, were initially grouped into 106 clusters using an adaptive resonance theory-based

160   neural network algorithm (ART-2a) with a vigilance factor of 0.8, learning rate of 0.05, and 20

161   iterations (Song et al., 1999). Then, by manually combining similar clusters, four primary types

162   of Fe-containing aerosols were obtained, including Fe-rich, Fe internally mixed with mineral

163   dust species (Fe-dust), Fe internally mixed with EC (Fe-EC), and Fe internally mixed with V

164   (Fe-V).

165

166   **3 Result and discussion**

167   **3.1 Characteristics and potential sources of the Fe-containing particle types**

168   The averaged mass spectra of the four Fe-containing types are shown in Figure 1. One common

169   feature was that the four Fe-containing particle types were internally mixed with secondary

170   inorganic ions such as sulfate (m/z -97[HSO_4]$^-$) and/or nitrate (m/z -46[NO_2]$^-$ or -62[NO_3]$^-$).

171   This suggests that the Fe-containing aerosols experienced atmospheric aging processes during

172   long-range transport.

173   The Fe-rich type exhibited the highest peak at m/z 56 Fe as well as sulfate and nitrate, which

174   was the largest fraction of Fe-containing particles, and contributed approximately 80% to the

175   cloud residues, interstitial particles, and cloud-free particles (Figure 2). The crustal elements

176   were rarely detected in the Fe-rich type, suggesting a nonmineral dust source. The Fe-rich type

177   was unlikely to be caused by biomass burning sources due to the weak potassium (m/z 39[K]$^+$)

178 peak (Bi et al. 2011). Lithium (m/z 7[Li]$^+$) was found to account for 7% of the Fe-rich type,

179 implying a partial contribution from fly ash as suggested by Furutani et al. (2011). Zhang et al.

180 (2014) considered that the Fe-rich particles were mostly produced by the iron/steel industry

181 from Shanghai in eastern China. In this study, a steel production site with an annual yield of 6.5

182 million tons was located approximately 60 km east of the sampling site. The Fe-rich type

183 detected here was most likely from industrial activities.

184   The Fe-dust type was mainly composed of mineral dust peaks including [Al]$^+$ (m/z 27), [Ca]$^+$

185 (m/z 40), [SiO$_3$]$^-$ (m/z -76), and [PO$_3$]$^-$ (m/z -79) (Figure 1), which accounted for 12-15% of the

186 cloud residues, interstitial particles, and cloud-free particles (Figure 2). However, no clear

187 enhancement of the Fe-dust aerosols was detected in the micron size (Figure S2). The micron

188 Fe-dust aerosols might have already been deposited over long-distance transport. Additionally,

189 the Fe-dust type may have occupied a larger size that could not be detected by the SPAMS.

190   The Fe-EC type was characterized by EC cluster ions (e.g., m/z $\pm$12[C]$^{+/-}$, $\pm$24[C$_2$]$^{+/-}$, $\pm$

191 [36C$_3$]$^{+/-}$, $\pm$48[C$_4$]$^{+/-}$, $\pm$[60C$_5$]$^{+/-}$) as well as strong sulfate (Figure 1). The internal mixture

192 of Fe-containing particles with EC was also observed in the Asian outflow atmosphere, mainly

193 due to the contribution from fossil fuel combustion in China (Furutani et al., 2011). The Fe-V

194 type showed the intense [Fe]$^+$ and [V]$^+$ (m/z 51) or vanadium oxide (m/z 67[VO]$^+$) peaks

195 (Figure 1). The Fe-V type was possibly related to residual fuel oil combustion sources, such as

196 ships and refineries (Furutani et al., 2011; Zhang et al., 2014; Dall'Osto et al., 2016). The Fe-

197 EC and Fe-V types were minor contributors (below 5%) in this study (Figure 2).

198

199 **3.2 The impact of cloud processing on secondary inorganic species in the Fe-containing**

200 **cloud residues**

201 Sulfate, nitrate, chloride, and ammonium were the most common secondary inorganic species

202 produced by aqueous reactions. Comparisons of these secondary inorganic species between Fe-

203 containing cloud residues, interstitial particles and cloud-free particles showed the impact of

204 cloud processing or aqueous phases on the formation of these species associated with Fe-

205 containing particles. Comparisons during daytime (local time 0800-1900) and nighttime (local

206 time 2000-0700) were also performed to investigate the irradiation effect. However, due to the

207 low number of particles detected, the Fe-EC and Fe-V particle types were not analyzed in this

208 section. Note that variation in the meteorological conditions may influence the comparisons.

209 The number fractions (NFs) of sulfate in the Fe-containing cloud residues (93%) and

210 interstitial particles (92%) were lower than those in the cloud-free particles (96%), as shown in

211 Figure 3. The sulfate peak area, proportional to mass, in the Fe-containing cloud residues and

212 interstitial particles were 0.96 and 0.85 times than that in the cloud-free particles. The NFs of

213 sulfate in the non-Fe cloud residues and interstitial particles were also not observed to enhance

214 relative to the non-Fe cloud-free particles (87-88% versus 92%). Several field studies also failed

215 to find the increased NF or mass fraction of sulfate in cloud residues or interstitial particles

216 (Drewnick et al., 2007; Twohy and Anderson, 2008; Schneider et al., 2017). The cause for these

217 observations remained unknown. In this study, an extremely high NF of sulfate was measured

218 in the Fe-containing cloud-free particles, which makes it hard to find the minor changes after

219 the particles experienced cloud events. It was worth noting that the Fe-containing particles

220 might experience one or more cloud processes prior to arrival at the observed site, wherein

221 sulfate may have accumulated on the Fe-containing particles. Low SO_2 level (below 5 ppb) in

222   the observed site may also limit the formation of sulfate. Thus, we speculated that the

223   contribution from the in-cloud formation of sulfate was relatively small compared to the total

224   amount of sulfate in the Fe-containing cloud-free particles in this study.

225   The NFs of nitrate in the Fe-containing cloud residues (86%) and interstitial particles (89%)

226   were enhanced in comparison to the cloud-free particles (76%) (Figure 3). The enhancement of

227   nitrate during cloud processing can be attributed to the partitioning from gaseous HNO_3 into

228   the aqueous phase and/or the heterogeneous reaction of N_2O_5 (Hayden et al., 2008; Chang et al.,

229   2011; Schneider et al., 2017). Photochemical reactions probably played a vital role in nitrate

230   formation (Pathak et al., 2009), leading to the increased NF of nitrate in the Fe-containing

231   cloud-free particles during daytime (Figure 4b). However, in the case of the Fe-containing cloud

232   residues, there was no distinct change in NF of nitrate between daytime and nighttime (Figure

233   4b), reflecting that the in-cloud formation of nitrate was less affected by photochemical

234   reactions. The higher NF of nitrate in the Fe-dust cloud residues was compared with the Fe-rich

235   cloud residues, despite a similar NF of nitrate observed in the two Fe-containing cloud-free

236   particle types (Figure 4b). This can be explained by the fact that gaseous HNO_3 would be

237   neutralized upon reaction with alkaline-rich (e.g., Ca) particles in the Fe-dust cloud residues

238   during cloud processing (Matsuki et al., 2010).

239   Higher NFs of chloride were found in the Fe-containing cloud residues and interstitial

240   particles compared to the cloud-free particles (16-13% versus 6%) (Figure 3). Sellegri et al.

241   (2003) observed that 80% of chloride in the aqueous phase originated from volatile gaseous

242   chloride (i.e., HCl) during cloud processing. The enhancement of chloride during cloud

243   processing was unlikely to have resulted from the invasion of sea salt particles, because the

244   related sea salt peaks (e.g., m/z 81 or 83[Na_2Cl]$^{+}$) were barely detected in the Fe-containing

245   cloud residues. Only 115 sea salt particles were obtained in the Non-Fe cloud residues,

246   suggesting less gaseous HCl was released from aged sea salt particles during cloud processing.

247   There was no change in the NF of chloride in the Fe-containing cloud residues during either

248   daytime or nighttime, although enhanced chloride levels were found in the Fe-containing cloud-

249   free particles during daytime (Figure 4c). This result suggests that the amount of in-cloud

250   chloride formation could overwhelm the simultaneous irradiation effect. A significant feature

251   was also found in that the NF of chloride in the Fe-dust cloud residues was much higher than

252   that in the Fe-rich cloud residues (45% versus 12%) (Figure 4c). Relative to sulfate and nitrate,

253   chloride showed a highly internally mixed state with Ca particles (Figure S3), indicating that

254   the Ca-rich particles in the Fe-dust cloud residues were responsible for the in-cloud formation

255   of chloride. Despite lower amounts of Ca particles in the Fe-rich cloud residues, the enhanced

256   NF of chloride was obvious (Figure 4c). This was likely attributed to the uptake of volatile

257   gaseous chloride (i.e., HCl) over simple physical sorption due to the high water solubility of

258   gaseous HCl (Sellegri et al., 2003).

259   The NFs of ammonium in the Fe-containing cloud residues (35%) and interstitial particles

260   (34%) were slightly higher than that in the cloud-free particles (30%) (Figure 3). Nearly 100%

261   of ammonium was found to be internally mixed with sulfate and/or nitrate in the Fe-rich cloud

262   residues. The increased NF of ammonium in the Fe-rich cloud residues was expected to take up

263   gaseous NH_3 to neutralize the secondary acids. Analogously, most ammonium in the Fe-dust

264   cloud residues was also internally mixed with sulfate and/or nitrate. The secondary acids

265   accumulated on the Fe-Dust cloud residues might be a sink for NH_3 (Sullivan et al., 2007; Nie

266   et al., 2012). However, enhancement of ammonium in the Fe-dust cloud residues was only

267   measured during nighttime (Figure 4d). Compared to nighttime, the increased ammonium in

268   the Fe-dust cloud-free particles was the combined result of the enhancement of nitrate and

269   chloride during daytime (Figure 4d). This process might lead to a minor change in the NF of

270   ammonium between the Fe-dust cloud residues and cloud-free particles during daytime.

271

272   **3.3 The impact of cloud processing on oxalate precursors and oxalate in the Fe-containing**

273   **cloud residues**

274   The aqueous oxidation pathway of organic precursors was an important contributor to the in-

275   cloud formation of oxalate (Sorooshian et al., 2007; Zhang et al., 2017). Acetate (at m/z -59

276   [$C_2H_3O_2$]$^-$), methylglyoxal (m/z -71 [$C_3H_3O_2$]$^-$), glyoxylate (m/z -73 [C_2HO_3]$^-$), pyruvate (m/z

277   -87 [$C_3H_3O_3$]$^-$), malonate (m/z -103 [$C_3H_3O_4$]$^-$), and succinate (m/z -117 [$C_4H_5O_4$]$^-$) had been

278   suggested as the main precursors for the formation of oxalate in the atmospheric aqueous phase

279   (Ervens et al., 2004; Lim et al., 2005; Sorooshian et al., 2006). Increased NFs of these

280   precursors were clearly identified in the Fe-containing cloud residues (38%) and interstitial

281   particles (35%) compared to cloud-free particles (26%) (Figure 3). These findings indicate the

282   contribution of cloud processing to the formation of oxalate precursors. Photochemical

283   reactions were another major pathway to form oxalate precursors (Kawamura and Bikkina,

284   2016). Although enhancement of the oxalate precursors was observed in the Fe-containing

285   cloud-free particles during daytime, no variation in NF of the oxalate precursors was found in

286   the Fe-containing cloud residues during either daytime or nighttime (Figure 4e). Therefore, the

287   in-cloud formation of the oxalate precursors is less likely to be influenced by photochemical

288   reactions. Interestingly, these precursors presented in 62% of the Fe-dust cloud residues, which

289   was much higher than 35% of the Fe-rich cloud residues (Figure 4e). A similar trend was also

290   found during the cloud-free periods (43% versus 23%) (Figure 4e). These findings suggest that

291   the oxalate precursors would readily enrich in the Fe-dust particles.

292   The NFs of oxalate in the Fe-containing cloud residues (45%) and interstitial particles (38%)

293   were higher than that in the cloud-free particles (25%) (Figure 3). Only slightly enhanced NFs

294   of oxalate without its precursors were found for the Fe-containing cloud residues (15%) and

295   interstitial particles (13%) in comparison to the cloud-free particles (10%) (Figure S4). This

296   possibly resulted from gaseous oxalic acid partitioning into cloud droplets (Sellegri et al., 2003).

297   It should be mentioned here that such an enhancement of oxalate may be related to other

298   precursors (e.g., glutarate) that were not considered in this study. On the other hand, oxalate

299   that was internally mixed with its precursors accounted for 30% and 25% of the Fe-containing

300   cloud residues and interstitial particles, respectively, which were higher than the amount in the

301   cloud-free particles (16%) (Figure S4). Similarly, the oxalate peak area was enhanced in the Fe-

302   containing cloud residues and interstitial particles when it was internally mixed with its

303   precursors (Figure S5). These results indicate that the presence of oxalate precursors would

304   enhance the in-cloud formation of oxalate, mostly via the aqueous oxidation of oxalate

305   precursors (Ervens et al., 2004; Sorooshian et al., 2006). Compared with the Fe-rich cloud

306   residues, the higher NF of oxalate in the Fe-dust cloud residues (Figure 4f) might be related to

307   the plentiful precursors in the Fe-dust cloud residues (Figure 4e). Interestingly, a lower NF of

308   oxalate in the Fe-containing cloud residues was measured during daytime relative to nighttime,

309   indicating the photolysis of Fe-oxalate complexes (Figure 4f). This phenomenon differed

310 greatly from the in-cloud formation of nitrate, chloride, and oxalate precursors in that their NF

311 had no obvious change during both daytime and nighttime. The lower NF of oxalate in the Fe-

312 containing cloud residues during daytime also implies that the photolysis of Fe-oxalate

313 complexes could overwhelm the in-cloud formation of oxalate during the day.

314   The Fenton reaction ($Fe^{2+} + H_2O_2 \rightarrow Fe^{3+} + OH^- + \cdot OH$) would yield OH-radicals, which

315 promote the conversion of the precursors to oxalate during cloud processing (Lim et al., 2010).

316 Obviously, the higher NF of oxalate in the Fe-containing cloud residues was compared with the

317 non-Fe cloud residues (45% versus 7%) (Figure S6). Moreover, a peak area ratio of oxalate to

318 its precursors was enhanced in the Fe-containing cloud residues relative to non-Fe cloud

319 residues (Figure 5a). These findings supported the role of the Fenton reaction in the conversion

320 of the precursors to oxalate during cloud processing. Sorooshian et al. (2007) observed that

321 oxalate was more efficiently produced from aqueous oxidation of glyoxylate with higher cloud

322 liquid water content, corresponding to higher cloud droplet pH values. Relative to Fe-

323 containing interstitial particles, an increased peak area ratio of oxalate to its precursors in the

324 cloud residues (Figure 5a) might be due to their higher liquid water content. Moreover, in the

325 presence of ammonium, the peak area ratio of oxalate to its precursors was also enhanced in the

326 Fe-containing cloud residues (Figure S7). The enhanced peak area ratio of oxalate to its

327 precursors in the Fe-dust cloud residues at night (Figure 5b) was likely due to the enhancement

328 of ammonium. Furthermore, nearly 90% of oxalate was found to be internally mixed with

329 ammonium in the Fe-dust cloud residues during nighttime. Ortiz-Montalvo et al. (2013)

330 considered that the formation of ammonium oxalate would substantially reduce the vapor

331 pressure of oxalate, enhancing the yield of oxalate during cloud processing. During the daytime,

332   the decreased peak area ratio of oxalate to its precursors mostly resulted from the degradation

333   of oxalate associated with photolysis of Fe-oxalate complexes.

334

335   **3.4 Mixing state of the Fe-containing cloud residues**

336   Figure 6 displays the number fraction of various species in the four Fe-containing cloud residual

337   types. Abundant sulfate was found in the Fe-rich (94%), Fe-dust (85%), Fe-EC (92%) and Fe-

338   V (98%) cloud residues. Substantial sulfate in the Fe-containing particles was also observed

339   over East Asia (Furutani et al., 2011; Moffet et al., 2012; Li et al., 2013). Despite no

340   significantly increased sulfate in Fe-containing particles during cloud processing, the

341   substantial sulfate observed here was expected due to the likely high levels of SO_2 encountered

342   during long-distance transport. High amounts (82-92%) of nitrate were observed in the Fe-

343   containing cloud residues except for the Fe-EC type (59%). However, a relatively high NF of

344   ammonium was obtained in the Fe-EC cloud residues (62%) compared to the other Fe-

345   containing cloud residual types (33-41%). This implies that ammonium in the Fe-EC particles

346   was likely in the form of ammonium sulfate, rather than ammonium nitrate. It should be noted

347   here that the evaporation chamber of the GCVI may lead to a depletion of ammonium nitrate

348   in the Fe-EC cloud residues (Hayden et al., 2008). The higher NF of chloride was found in the

349   Fe-dust cloud residues (45%) relative to the other Fe-containing cloud residual types (12-14%).

350   As discussed above, the Ca-rich particles in the Fe-dust type contributed considerably to the in-

351   cloud formation of chloride. Oxalate accounted for 45-51% of the Fe-rich, Fe-V, and Fe-dust

352   cloud residues, which was much higher than the oxalate found in Fe-EC cloud residues (19%).

353   The less abundant oxalate in the Fe-EC cloud residues might be restricted by the low NF of the

354   oxalate precursors.

355

356   **4 Atmospheric implications**

357   Previous laboratory and modeling studies focused on the cloud processing of Fe-containing

358   particles from dust sources (Hand et al., 2004; Mahowald et al., 2005; Shi et al., 2009). Some

359   modeling studies argued that the combustion Fe sources should be taken into account over East

360   Asia (Luo et al., 2008; Ito, 2015). Several field studies also confirmed the importance of

361   combustion sources to the Fe-containing particles over East Asia (Furutani et al., 2011; Moffet

362   et al., 2012; Zhang et al., 2014). This study includes the first report of the abundant Fe-rich

363   particles related to the participation of combustion sources in cloud processing over East Asia.

364   Luo et al. (2008) performed a modeling calculation to estimate the influence of atmospheric

365   process on soluble Fe by assuming that cloud processing had sufficient acidic species to process

366   more Fe soluble. However, they did not definite the specific acid types. In the current study, the

367   in-cloud formation of nitrate and chloride was enhanced in the Fe-dust type relative to the Fe-

368   rich type. Laboratory studies also showed that Fe dissolution in the HCl solution differed from

369   that in the H_2SO_4 and HNO_3 solutions (Fu et al., 2010; Rubasinghege et al., 2010). In order to

370   accurately predict bioavailable Fe during cloud processing, the impact of different acids on Fe

371   dissolution in varied Fe types might be considered for future modeling study.

372   Modeling calculations showed that relative to proton-promoted Fe dissolution, the addition

373   of oxalate accompanied with photolysis of Fe-oxalate complexes in aqueous chemistry more

374   than doubled the soluble Fe deposition from combustion sources in global oceanic regions (Ito,

375   2015). Our data showed that aqueous-phase oxidation of the oxalate precursors was an

376   important contributor to the in-cloud formation of oxalate in the Fe-rich particles. The Fenton

377   reaction would further promote the conversion of the oxalate precursors to oxalate in the Fe-

378   rich particles during cloud processing. At the same time, the photolysis of Fe-oxalate complexes

379   in the Fe-rich cloud residues also existed. These results supported the role of oxalate in aqueous

380   chemistry in soluble Fe deposition from combustion sources. However, the modeling study

381   assumed that oxalate was entirely mixed with Fe-containing particles from combustion sources

382   (Ito, 2015). In this work, nearly 50% of the Fe-rich cloud residues contained only oxalate. The

383   relative low number of oxalate in the Fe-rich cloud residues may reduce or suppress the

384   contribution of oxalate to the Fe dissolution during cloud processing (Ito, 2015). Ito (2015) also

385   proposed that the formation of Ca-oxalate complexes may reduce the availability of oxalate for

386   Fe-oxalate complexes, leading to the suppression of Fe dissolution. Less content (13%) of Ca-

387   containing particles in the Fe-rich type suggests that Ca-oxalate complexes are a minor

388   contributor to the Fe-rich type. Hence, the suppression of Fe dissolution due to Ca-oxalate

389   complexes in the Fe-rich type was not important during cloud processing in this study.

390

391   **5 Conclusions**

392   The Fe-rich type was dominant in the Fe-containing cloud residues, highlighting the major

393   contribution from combustion sources. This work also identified the in-cloud formation of

394   secondary species on the Fe-containing particles. No enhancement of sulfate was found in the

395   Fe-containing cloud residues. The enhancement of nitrate and chloride in the Fe-containing

396   particles was produced via partitioning and heterogeneous/aqueous chemistry of gaseous HNO_3

397   and HCl or other precursors. The in-cloud formation of oxalate was mostly attributed to the

398   aqueous oxidation of its precursors. The Fenton reaction and presence of ammonium species

399   further facilitated the in-cloud formation of oxalate. These results have important implications

400   for improving the modeling of atmospheric processes of aerosol Fe and evaluating Fe

401   bioavailability during cloud processing.

402

403   **Acknowledgements**

404   This work was supported by the National Key Research and Development Program of China

405   (2017YFC0210104), the National Nature Science Foundation of China (No. 41877307,

406   41775124 and 41805103), the Foundation for Leading Talents of the Guangdong Province

407   Government, and the State Key Laboratory of Organic Geochemistry (SKLOGA201603A). MJ

408   Tang would like to thank Chinese Academy of Sciences international collaborative project (No.

409   132744KYSB20160036).

410

411   **References**

412   Abbaspour, N., Hurrell, R., and Kelishadi, R.: Review on iron and its importance for human

413   health, J. Res. Med. Sci., 19, 164-174, 2014.

414   Bhave, P.V., Allen, J.O., Morrcal, B.D., Fergenson, D.P., Cass, G.R., and Prather, K. A.: A field-

415   based approach for determining atofms instrument sensitivities to ammonium and nitrate,

416   Environ. Sci. Technol., 36, 4868-4879, https://doi.org/10.1021/es015823i, 2002.

417   Bi, X., Lin, Q., Peng, L., Zhang, G., Wang, X., Brechtel, F.J., Chen, D., Li, M., Peng, P.A.,

418   Sheng, G., and Zhou, Z.: In situ detection of the chemistry of individual fog droplet

419   residues in the Pearl River Delta region, China, J. Geophys. Res. Atmos., 121, 9105-9116,

420   https://doi.org/10.1002/2016JD024886, 2016.

421   Bi, X., Zhang, G., Li, L., Wang, X., Li, M., Sheng, G., Fu, J., and Zhou, Z.: Mixing state of

422   biomass burning particles by single particle aerosol mass spectrometer in the urban area

423   of PRD, China, Atmos. Environ., 45, 3447-3453,

424   https://doi.org/10.1016/j.atmosenv.2011.03.034, 2011.

425   Chang, W.L., Bhave, P.V., Brown, S.S., Riemer, N., Stutz, J., and Dabdub, D.: Heterogeneous

426   atmospheric chemistry, ambient measurements, and model calculations of N_2O_5: A review,

427   Aerosol Sci. Tech., 45, 665-695, https://doi.org/10.1080/02786826.2010.551672, 2011.

428   Cheng, C., Li, M., Chan, C.K., Tong, H., Chen, C., Chen, D., Wu, D., Li, L., Wu, C., Cheng, P.,

429   Gao, W., Huang, Z., Li, X., Zhang, Z., Fu, Z., Bi, Y., and Zhou, Z.: Mixing state of oxalic

430   acid containing particles in the rural area of Pearl River Delta, China: implications for the

431   formation mechanism of oxalic acid, Atmos. Chem. Phys., 17, 9519-9533,

432   https://doi.org/10.5194/acp-17-9519-2017, 2017.

433   Costa, D.L., and Dreher, K.L.: Bioavailable transition metals in particulate matter mediate

434   cardiopulmonary injury in healthy and compromised animalmodels, Environ. Health

435   Perspect., 105, 1053-1060, https://doi.org/10.1289/ehp.97105s51053, 1997.

436   Dall'Osto, M., Beddows, D.C., Harrison, R.M., and Onat, B.: Fine iron aerosols are internally

437   mixed with nitrate in the urban European atmosphere, Environ. Sci. Technol., 50, 4212-

438   4220, https://doi.org/10.1021/acs.est.6b01127, 2016.

439   Dall'Osto, M., Harrison, R.M., Highwood, E.J., O'Dowd, C., Ceburnis, D., Querol, X., and

440   Achterberg, E.P.: Variation of the mixing state of Saharan dust particles with atmospheric

441   transport, Atmos. Environ., 44, 3135-3146,

442   https://doi.org/10.1016/j.atmosenv.2010.05.030, 2010.

Drewnick, F., Schneider, J., Hings, S.S., Hock, N., Noone, K., Targino, A., Weimer, S., and
Borrmann, S.: Measurement of ambient, interstitial, and residual aerosol particles on a
mountaintop site in central Sweden using an aerosol mass spectrometer and a CVI, J.
Atmos. Chem., 56, 1-20, https://doi.org/10.1007/s10874-006-9036-8, 2007.

Ervens, B., Feingold, G., Frost, G. J., and Kreidenweis, S. M.: A modeling study of aqueous
production of dicarboxylic acids: 1. chemical pathways and speciated organic mass
production, J. Geophys. Res. Atmos., 109, D15205,
https://doi.org/10.1029/2003JD004387, 2004.

Ervens, B., Turpin, B., and Weber, R.: Secondary organic aerosol formation in cloud droplets
and aqueous particles (aqSOA): a review of laboratory, field and model studies, Atmos.
Chem. Phys., 11, 11069-11102, https://doi.org/10.5194/acp-11-11069-2011, 2011.

Fu, H., Cwiertny, D. M., Carmichael, G. R., Scherer, M. M., and Grassian, V. H.: Photoreductive
dissolution of Fe-containing mineral dust particles in acidic media, J. Geophys. Res.
Atmos., 115, D11304, https://doi.org/ 10.1029/2009JD012702, 2010.

Furutani, H., Jung, J., Miura, K., Takami, A., Kato, S., Kajii, Y., and Uematsu, M.: Single-
particle chemical characterization and source apportionment of iron-containing
atmospheric aerosols in Asian outflow, J. Geophys. Res. Atmos., 116, D18204,
https://doi.org/10.1029/2011JD015867, 2011.

Hand, J.L., Mahowald, N. M., Chen, Y., Siefert, R.L., Luo, C., Subramaniam, A., and Fung, I.:
Estimates of atmospheric-processed soluble iron from observations and a global mineral
aerosol model: biogeochemical implications, J. Geophys. Res. Atmos., 109, D17205,
https://doi.org/10.1029/2004JD004574, 2004.

465 Harris, E., Sinha, B., van Pinxteren, D., Tilgner, A., Fomba, K.W., Schneider, J., Roth, A.,

466   Gnauk, T., Fahlbusch, B., Mertes, S., Lee, T., Collett, J., Foley, S., Borrmann, S., and

467   Herrmann., H.: Enhanced role of transition metal ion catalysis during in-cloud oxidation

468   of SO_2, Science, 340, 727-730, https://doi.org/10.1126/science.1230911, 2013.

469 Hayden, K.L., Macdonald, A.M., Gong, W., Toom-Sauntry, D., Anlauf, K.G., Leithead, A., Li,

470   S.M., Leaitch, W.R., and Noone, K.: Cloud processing of nitrate, J. Geophys. Res. Atmos.,

471   113, D18201, https://doi.org/10.1029/2007JD009732, 2008.

472 Ito, A.: Atmospheric processing of combustion aerosols as a source of bioavailable iron,

473   Environ. Sci. Technol. Lett., 2, 70-75, https://doi.org/10.1021/acs.estlett.5b00007, 2015.

474 Jickells, T.D., An, Z.S., Andersen, K.K., Baker, A.R., Bergametti, G., Brooks, N., Cao, J.J.,

475   Boyd, P.W., Duce, R.A., Hunter, K.A., Kawahata, H., Kubilay, N., LaRoche, J., Liss, P.S.,

476   Mahowald, N., Prospero, J.M., Ridgwell, A.J., Tegen, I., and Torres, R.: Global iron

477   connections between desert dust, ocean biogeochemistry, and climate, Science, 308, 67-

478   71, https://doi.org/10.1126/science.1105959, 2005.

479 Kawamura, K., and Bikkina, S.: A review of dicarboxylic acids and related compounds in

480   atmospheric aerosols: molecular distributions, sources and transformation, Atmos. Res.,

481   170, 140-160, https://doi.org/10.1016/j.atmosres.2015.11.018, 2016.

482 Li, L., Huang, Z., Dong, J., Li, M., Gao, W., Nian, H., Fu, Z., Zhang, G., Bi, X., and Cheng, P.:

483   Real time bipolar time-of-flight mass spectrometer for analyzing single aerosol particles,

484   Int. J. Mass Spectrom., 303, 118-124, https://doi.org/10.1016/j.ijms.2011.01.017, 2011.

485 Li, W., Wang, T., Zhou, S., Lee, S., Huang, Y., Gao, Y., and Wang, W.: Microscopic observation

486   of metal-containing particles from Chinese continental outflow observed from a non-

487   industrial site, Environ. Sci. Technol., 47, 9124-9131, https://doi.org/10.1021/es400109q,

488   2013.

489 Lim, H.J., Carlton, A.G., and Turpin, B.J.: Isoprene forms secondary organic aerosol through

490   cloud processing: Model simulations, Environ. Sci. Technol., 39, 4441-4446,

491   https://doi.org/10.1021/es048039h, 2005,

492 Lim, Y.B., Tan, Y., Perri, M.J., Seitzinger, S.P., and Turpin, B.J.: Aqueous chemistry and its role

493   in secondary organic aerosol (SOA) formation, Atmos. Chem. Phys., 10, 10521-10539,

494   https://doi.org/10.5194/acp-10-10521-2010, 2010.

495 Lin, Q., Zhang, G., Peng, L., Bi, X., Wang, X., Brechtel, F.J., Li, M., Chen, D., Peng, P., Sheng,

496   G., and Zhou, Z.: In situ chemical composition measurement of individual cloud residue

497   particles at a mountain site, southern China, Atmos, Chem. Phys., 17, 8473-8488,

498   https://doi.org/10.5194/acp-17-8473-2017, 2017.

499 Luo, C., Mahowald, N., Bond, T., Chuang, P.Y., Artaxo, P., Siefert, R., Chen, Y., and Schauer,

500   J.: Combustion iron distribution and deposition, Global Biogeochem. Cycles, 22, GB1012,

501   https://doi.org/10.1029/2007GB002964, 2008.

502 Mahowald, N.M., Baker, A.R., Bergametti, G., Brooks, N., Duce, R. A., Jickells, T. ., Kubilay,

503   N., Prospero, J.M., and Tegen, I.: Atmospheric global dust cycle and iron inputs to the

504   ocean, Global Biogeochem. Cycles, 19, GB4025, https://doi.org/10.1029/2004GB002402,

505   2005.

506 Matsuki, A., Schwarzenboeck, A., Venzac, H., Laj, P., Crumeyrolle, S., and Gomes, L.: Cloud

507   processing of mineral dust: direct comparison of cloud residual and clear sky particles

508   during AMMA aircraft campaign in summer 2006, Atmos. Chem. Phys., 10, 1057-1069,

509   https://doi.org/10.5194/acp-10-1057-2010, 2010.

510   Moffet, R.C., Furutani, H., Rödel, T.C., Henn, T.R., Sprau, P.O., Laskin, A., Uematsu, M., and

511   Gilles, M.K.: Iron speciation and mixing in single aerosol particles from the Asian

512   continental   outflow,   J.   Geophys.   Res.   Atmos.,   117,   D07204,

513   https://doi.org/10.1029/2011JD016746, 2012.

514   Nie, W., Wang, T., Xue, L. K., and Ding, A. J.: Asian dust storm observed at a rural mountain

515   site in southern china: chemical evolution and heterogeneous photochemistry, Atmos.

516   Chem. Phys., 12, 11985-11995, https://doi.org/10.5194/acp-12-11985-2012, 2012.

517   Ortiz-Montalvo, D.L., Häkkinen, S.A.K., Schwier, A.N., Yong, B.L., Mcneill, V.F., and Turpin,

518   B. J.: Ammonium addition (and aerosol pH) has a dramatic impact on the volatility and

519   yield of glyoxal secondary organic aerosol, Environ. Sci. Technol., 48, 255-262,

520   https://doi.org/10.1021/es4035667, 2013.

521   Pathak, R. K., Wu, W. S., and Wang, T.: Summertime $PM_{2.5}$ ionic species in four major cities

522   of china: nitrate formation in an ammonia-deficient atmosphere, Atmos. Chem. Phys., 9,

523   1711-1722, https://doi.org/10.5194/acp-9-1711-2009, 2009.

524   Pratt, K.A., Heymsfield, A.J., Twohy, C.H., Murphy, S.M., DeMott, P.J., Hudson, J.G.,

525   Subramanian, R., Wang, Z., Seinfeld, J.H., and Prather, K.A.: In Situ Chemical

526   Characterization of Aged Biomass-Burning Aerosols Impacting Cold Wave Clouds, J.

527   Atmos. Sci., 67, 2451-2468, https://doi.org/10.1175/2010JAS3330.1, 2010.

528   Pratt, K.A., Murphy, S. M., Subramanian, R., Demott, P.J., Kok, G.L., Campos, T., Rogers,

529   D.C., Prenni, A.J., Heymsfield, A.J., Seinfeld, J.H., and Prather, K.A.: Flight-based

530   chemical characterization of biomass burning aerosols within two prescribed burn smoke

plumes, Atmos. Chem. Phys., 11, 12549-2565, https://doi:10.5194/acp-11-12549-2011, 2011.

Rubasinghege, G., Lentz, R.W., Scherer, M.M., and Grassian, V.H.: Simulated atmospheric processing of iron oxyhydroxide minerals at low pH: roles of particle size and acid anion in iron dissolution, P. Natl. Acad. Sci. USA, 107, 6628-6633, https://doi.org/10.1073/pnas.0910809107, 2010.

Shi, Z., Krom, M.D., Bonneville, S., Baker, A.R., Jickells, T.D., and Benning, L.G.: Formation of iron nanoparticles and increase in iron reactivity in mineral dust during simulated cloud processing, Environ. Sci. Technol., 43, 6592-6596, https://doi.org/10.1021/es901294g, 2009.

Schneider, J., Mertes, S., van Pinxteren, D., Herrmann, H., and Borrmann, S.: Uptake of nitric acid, ammonia, and organics in orographic clouds: mass spectrometric analyses of droplet residual and interstitial aerosol particles, Atmos. Chem. Phys., 17, 1571-1593, https://doi.org/10.5194/acp-17-1571-2017, 2017.

See, S.W., Wang, Y.H., and Balasubramanian, R.: Contrasting reactive oxygen species and transition metal concentrations in combustion aerosols, Environ. Res., 103, 317-324, https://doi.org/10.1016/j.envres.2006.08.012, 2007.

Sedwick, P.N., Sholkovitz, E.R., and Church, T.M.: Impact of anthropogenic combustion emissions on the fractional solubility of aerosol iron: Evidence from the Sargasso Sea, Geochem. Geophys. Geosyst., 8, Q10Q06, https://doi.org/10.1029/2007GC001586, 2007.

Sellegri, K., Laj, P., Marinoni, A., Dupuy, R., Legrand, M., and Preunkert, S.: Contribution of gaseous and particulate species to droplet solute composition at the Puy de Dôme, France,

553   Atmos. Chem. Phys., 3, 1509-1522, https://doi.org/10.5194/acp-3-1509-2003, 2003.

554 Shingler, T., Dey, S., Sorooshian, A., Brechtel, F.J., Wang, Z., Metcalf, A., Coggon, M.,

555   Mülmenstädt, J., Russell, L.M., Jonsson, H.H., and Seinfeld, J.H.: Characterisation and

556   airborne deployment of a new counterflow virtual impactor inlet, Atmos. Meas. Tech., 5,

557   1259-1269, https://doi.org/10.5194/amt-5-1259-2012, 2012.

558 Song, X.H., Hopke, P.K., Fergenson, D.P., and Prather, K.A.: Classification of single particles

559   analyzed by ATOFMS using an artificial neural network, ART-2A, Anal. Chem., 71, 860-

560   865, https://doi.org/10.1021/ac9809682, 1999.

561 Sorooshian, A., Ng, N.L., Chan, A.W.H., Feingold, G., Flagan, R.C., and Seinfeld, J.H.:

562   Particulate organic acids and overall water-soluble aerosol composition measurements

563   from the 2006 Gulf of Mexico Atmospheric Composition and Climate Study (GoMACCS),

564   J. Geophys. Res. Atmos., 112, D13201, https://doi.org/10.1029/2007JD008537, 2007.

565 Sorooshian, A., Varutbangkul, V., Brechtel, F.J., Ervens, B., Feingold, G., Bahreini, R., Murphy,

566   S.M., Holloway, J. S., Atlas, E.L., Buzorius,G., Jonsson, H., Flagan, R.C., and Seinfeld,

567   J.H.: Oxalic acid in clear and cloudy atmospheres: analysis of data from international

568   consortium for atmospheric research on transport and transformation 2004, J. Geophys.

569   Res. Atmos., 111, D23S45, https://doi.org/10.1029/2005JD006880, 2006.

570 Sullivan, R., Guazzotti, S., Sodeman, D., and Prather, K.: Direct observations of the

571   atmospheric processing of Asian mineral dust, Atmos. Chem. Phys., 7, 1213-1236,

572   https://doi.org/10.5194/acp-7-1213-2007, 2007.

573 Sullivan, R., and Prather, K.: Investigations of the diurnal cycle and mixing state of oxalic acid

574   in individual particles in Asian aerosol outflow, Environ. Sci. Tech., 41, 8062-8069,

575 https://doi.org/10.1021/es071134g, 2007.

576 Tsai, I.C., Chen, J.P., Lin, P.Y., and Wang, W.C.: Sulfur cycle and sulfate radiative forcing

577 simulated from a coupled global climate-chemistry model, Atmos. Chem. Phys., 10, 3693-

578 3709, https://doi.org/10.5194/acp-10-3693-2010, 2010.

579 Twohy, C.H., and Anderson, J.R.: Droplet nuclei in non-precipitating clouds: composition and

580 size matter, Environ. Res. Lett., 3, 045002, doi:10.1088/1748-9326/3/4/045002, 2008.

581 Yang, F., Chen, H., Wang, X., Yang, X., Du, J., and Chen, J.: Single particle mass spectrometry

582 of oxalic acid in ambient aerosols in Shanghai: Mixing state and formation mechanism,

583 Atmos. Environ., 43, 3876-3882, https://doi.org/10.1016/j.atmosenv.2009.05.002, 2009.

584 Zhang, G., Bi, X., Lou, S., Li, L., Wang, H., Wang, X., Zhou, Z., Sheng, G., Fu, J., and Chen,

585 C.: Source and mixing state of iron-containing particles in Shanghai by individual particle

586 analysis, Chemosphere, 95, 9-16, https://doi.org/10.1016/j.chemosphere.2013.04.046,

587 2014.

588 Zhang, G., Lin, Q., Peng, L., Yang, Y., Fu, Y., Bi, X., Li, M., Chen, D., Chen, J., Cai, Z., Wang,

589 X., Peng, P., Sheng, G., and Zhou, Z.: Insight into the in-cloud formation of oxalate based

590 on in situ measurement by single particle mass spectrometry, Atmos. Chem. Phys., 17,

591 13891-13901, https://doi.org/10.5194/acp-17-13891-2017, 2017.

592 Figure captions:

593 Figure 1. The averaged mass spectra of the four Fe-containing types.

594 Figure 2. Number fraction of the four Fe-containing types in the Fe-containing cloud residues,

595 interstitial particles, and cloud-free particles during the whole study period. The uncertainties

596 were calculated assuming Poisson statistics for the analyzed particles (Pratt et al., 2010).

597 Figure 3. Comparison in number fractions of sulfate, nitrate, chloride, ammonium, oxalate

598 precursors, and oxalate between the Fe-containing cloud residues, interstitial particles and

599 cloud-free particles. Sulfate (m/z -97), nitrate (m/z -46 or -62), chloride (m/z -35 or -37),

600 ammonium (m/z 18), oxalate precursors (m/z -59 acetate or m/z -71 methylglyoxal or m/z -73

601 glyoxylate or m/z -87 pyruvate or m/z -103 malonate or m/z -117 succinate), and oxalate (m/z

602 -89).

603 Figure 4. Comparison in number fractions of sulfate (a), nitrate (b), chloride (c), and ammonium

604 (d), oxalate precursors (e), and oxalate (f) in the Fe-rich, Fe-dust, and all Fe-containing (total-

605 Fe) types between the cloud residues and cloud-free particles types and their difference during

606 daytime and nighttime. The comparison was not performed for the interstitial particles due to

607 the low number of detected particles.

608 Figure 5. Peak area ratio of oxalate to its precursors in the total-Fe and non-Fe types (a); Peak

609 area ratio of oxalate to its precursors in the Fe-rich, Fe-dust, total-Fe and non-Fe types during

610 daytime and nighttime (b).

611 Figure 6. Mixing state of the four Fe-containing cloud residues.
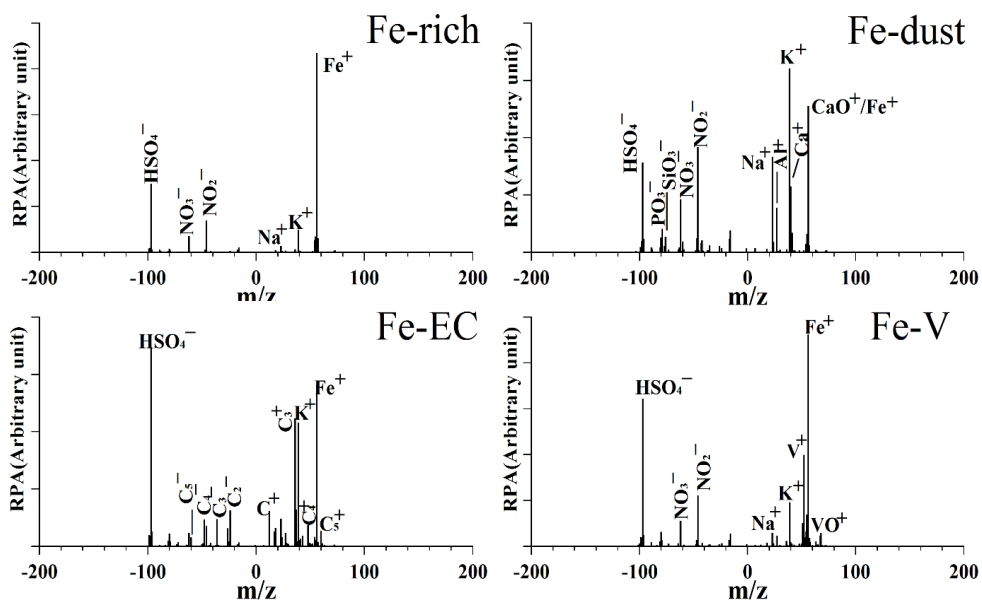
612

613   Figure 1.
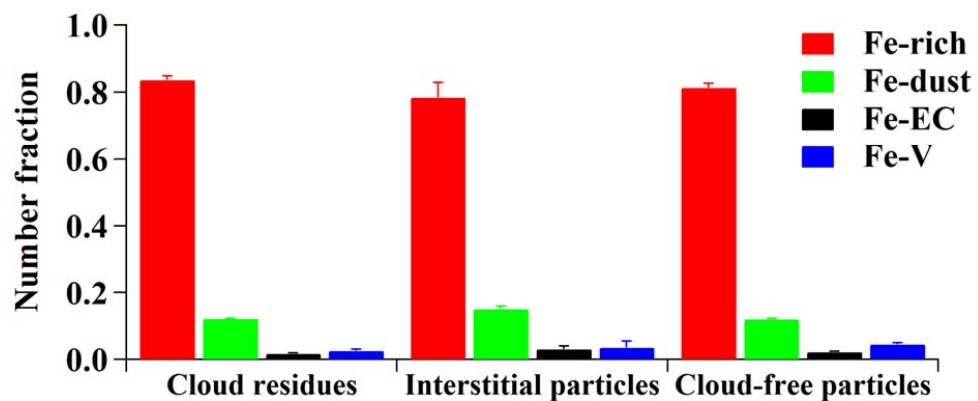
614

615   Figure 2.
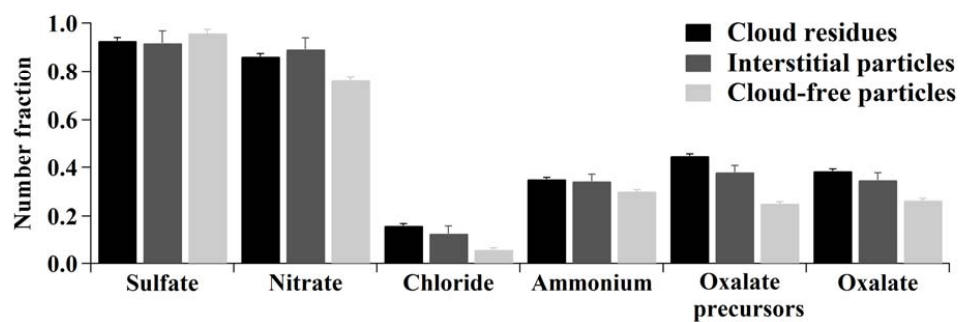
616

617   Figure 3.
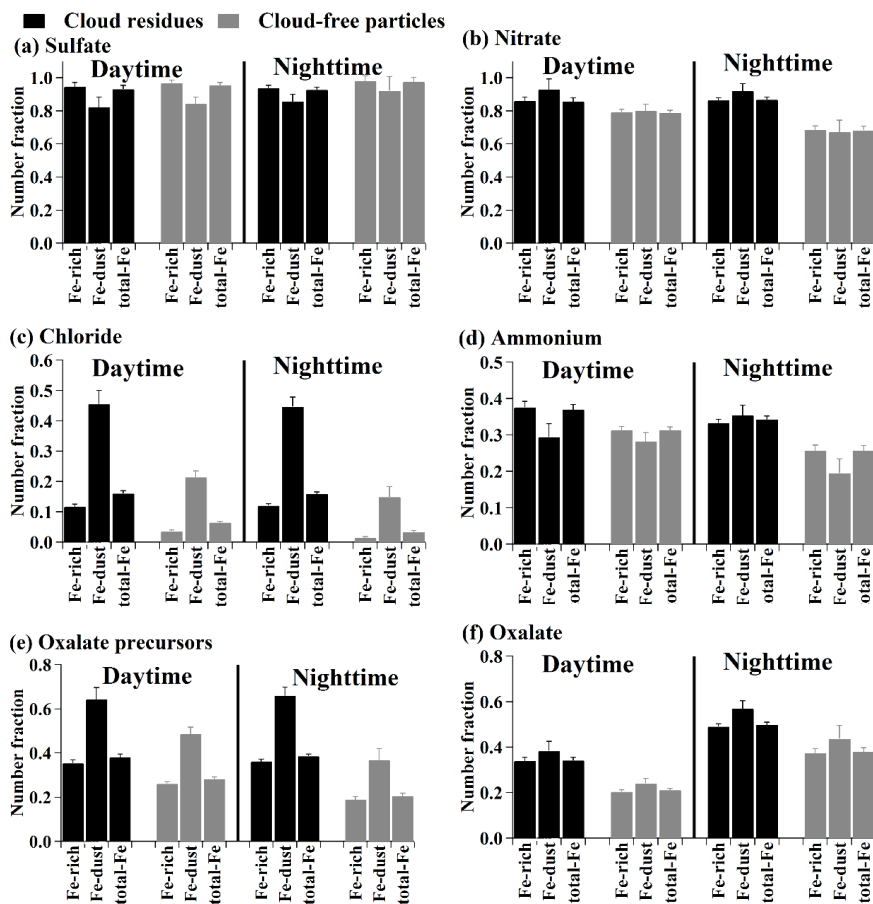
618

619   Figure 4.
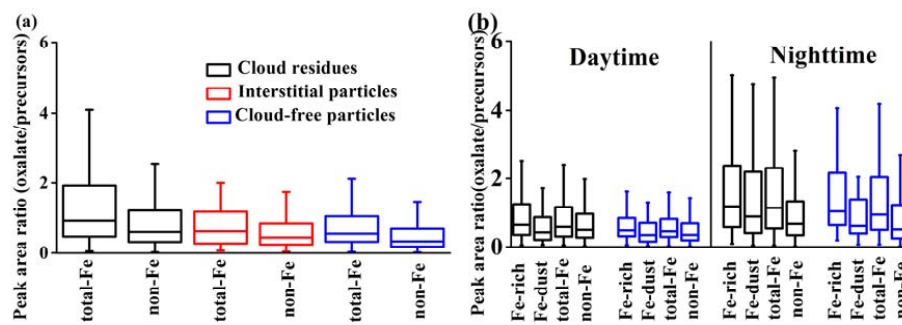
620

621   Figure 5.

622

623

624   Figure 6.